Microsystem Technologies (2022) 28:2429–2441
https://doi.org/10.1007/s00542-022-05372-y

TECHNICAL PAPER

Performance analysis of wideband microstrip patch antenna with amplified radiation

Anagh Sankar Das[1] · Aditya Goel[1] · Sangeeta Nakhate[1]

Received: 25 January 2021 / Accepted: 29 August 2022 / Published online: 12 September 2022

Abstract

The problem of narrow bandwidth is a major concern in general for MPA (Microstrip Patch Antenna). In this study, we have performed certain methods to enhance the antenna bandwidth by taking into consideration a proposed antenna and accordingly analyzed how it behaves by changing its various dimensions like patch length, antenna height, substrate thickness. The major objective of this analysis here, is to amplify the antenna bandwidth more than that of a normal patch antenna, which means that then this proposed structure could prove to be essential in a number of applications like WLAN (Wireless Local Area Network) and Bluetooth. The value of center frequency, for which a broad impedance bandwidth is observed for this antenna is 3 GHz that belongs to the S band (2–4 GHz) region. Simulations have been performed using Ansoft HFSS (High Frequency-Structure Simulator) simulation software which uses the FEM (Finite Element Method) procedure for solving its various operations. The patch antenna exhibits radiation intensity value of 14 dB which is projected at 0°. The proposed antenna, with the aid of numerical analysis of the patch measurements, undergoes a noticeable increment in the bandwidth that is visible at a particular resonant frequency, after comparisons are done with various other iterations. Furthermore, the value of the resonant frequency and the center frequency are both alike, i.e., 3 GHz. Also, VSWR (Voltage Standing Wave Ratio) for the antenna is near about 1. This means that the proposed structure has a great impedance match and it invariably plays a role in the antenna's wideband performance. Furthermore, the antenna possesses a gain of nearly 6 dB for that frequency accompanied by an absolutely symmetrical pattern of radiation, in addition to having an impedance bandwidth of 45.67%.

1 Introduction

Right from the advent of MPAs at around the earlier part of the 1970s, extensive researches were performed with the intention of improvement in the bandwidth. This can be augmented using familiar techniques, for instance enhancing substrate height (Mishra et al. 2015) or with the help of a lowly contrasted dielectric substrate (Radavaram and Pour 2019). Increment in bandwidth can also be done by locating parasitic patches either in a *non-identical* (Lee et al. 1987) or in the *same layer* (Chen et al. 1993), that produces stacked or coplanar configurations, individually. However, stacked configuration does not satisfy a few of the key features of these antennas, for instance low profile and the simple nature in fabrication (Gaharwar et al. 2021), while the coplanar configuration enhances the dimensions of the antenna. Detailed researches have been done to amplify the impedance bandwidth of the antennas which consists of a single-layer and various other studies were carried out that were solely based on wireless sensor communications (Ashraf 2020; Ashraf et al. 2020). Apart from this, research studies were concentrated on ascertaining the varied properties of these *U-slot patch antennas* (Lee et al. 2010; Weigand et al. 2003; Khan and Chatterjee 2016; Radavaram and Pour 2019; Naz et al. 2020; Deshmukh et al. 2021). Other than the U-slot design, other configurations were also proposed, for instance half *U-slot antennas* (Mak et al. 2003), *C-shaped* (Nguyen et al. 2021), *E-shaped* (Yang et al. 2001) and *ψ-shaped* (Sharma and Shafai 2009).

✉ Anagh Sankar Das
anaghsankardas@gmail.com

Aditya Goel
adityagoel2@rediffmail.com

Sangeeta Nakhate
sanmanit@gmail.com

[1] Department of Electronics and Communication Engineering, MANIT, Bhopal, India

Slot-loaded antennas are extensively useful in the field of wireless communications, as they are inexpensive in comparison to other antennas, and in addition to this, their low-profile nature (Saini and Kumar 2021) makes them invaluable. In general, patch antennas have lesser weights and are significantly in demand owing to the fact that their fabrication process is of simple-nature (Gopi et al. 2021) and on top of that their manufacturing is less tedious. These MPAs are fabricated on a PCB (Printed Circuit Board) using photolithographic techniques (Jung et al. 2020; Yunas et al. 2020; AL-Amoudi 2021). It primarily consists of a flat rectangular metallic sheet, that basically is the "patch" which we know about. It is then placed on top of a dielectric medium, which is the substrate, and beneath this layer there is an additional metal layer, which behaves like the ground plane. The entire radiation procedure happens as a result of the phenomenon of fringing where the virtual length of the patch seems larger than its actual physical length (Balanis 2016). A suitable antenna utilises a patch which is half of an ideal antenna wavelength. Usually, patches are abundant in a variety of sizes and figures. These can be elliptical in nature (Alani et al. 2020; Kaur and Malik 2021), even rectangular in shape (Ata et al. 2020; Bansal and Gupta 2020), or at times, circular (Ou et al. 2020; Prakasam et al. 2020). In addition to all these varieties, a variety of different shape modifications are in abundance. Furthermore, it is possible to create a patch antenna by creation of an arbitrary constant shape (Goudos et al. 2017), but keeping in mind that radiation must occur in an appropriate manner from the patch itself. Usually, ground planes that are virtually large in terms of electrical length (Balanis 2016), create pretty sound radiation patterns and are also responsible in enhancing the overall size of the antenna. Normally, it is quite a common occurrence where the ground plane measurement is slightly larger than patch measurement (Baudha et al. 2020). Assuming that the measurement of ground plane is nearly as close as possible to the dimensions of radiator (Dhara et al. 2021), a situation can arise where coupling can occur, thus producing current at the plane boundaries that can radiate as well. An antenna pattern is established, as a dual set of radiating metal elements combines together to create such an event (He and Li 2020). The process of radiation could be imagined as, that takes place as a result of certain slots that radiate from the topmost and the underlying layer, or at times even simultaneously as a result of current flowing through patch and ground layers.

Applications for the S-band (2–4 GHz) (Prajapati and Rawat 2020; Ghaffar et al. 2021) spectrum have recently attracted a lot of attention. These applications include satellites for communication, radars for precise weather prediction, radars used on ship surfaces, wireless local area network (WLAN), and also for its usage in multimedia, such as mobile TV and radio for satellites, etc. A variety of magnetically electrical dipole antenna designs with higher gain and bandwidth were examined thoroughly (Cai et al. 2020; Sun et al. 2019; Gao et al. 2019).

Upon careful evaluation of the state-of-the- literature, the authors have come to a conclusion that, enhancing the bandwidth of a patch antenna can make it far more effective for wideband applications and make it vastly useful for various wireless communication purposes. Keeping this in mind, a patch antenna is proposed, and its wideband performance is analysed. For this, we have prepared the proposed antenna design, which can generate a good wideband performance, contrary to a normal patch antenna, and in our efforts, we have included several number of iterations building up to the final model, via alterations in the patch measurements. In this endeavour, we have analysed the various performance parameters of our proposed structure like return loss, impedance bandwidth and radiation pattern, along with those iterations as well. Along with these, the plots of gain and VSWR were also studied which are important performance metrics for any patch antenna. Our main goal is to establish that, the proposed design could prove to be a good fit when compared to a conventional patch antenna with regards to its wideband performance and better radiation patterns. And for this reason, we have analysed the performance of our proposed antenna after implementing its design by checking the different performance metrics as mentioned above. The same was done with the help of a software named, *Ansoft HFSS* (Cendes 2016) which is mainly a simulation software based on antenna design.

2 Theory and formulae

An MPA (Microstrip Patch Antenna) can be easily established by carving slots (Guo et al. 1998) in favourable locations on the patch surface, which can be operated on a relatively smaller dielectric constant and a much broader substrate. The patch length measurement is always a vital factor as the procedure of fringing has an influence on the outcome of this parameter.

2.1 Patch length of proposed antenna

$$L_P \approx \frac{1}{2f_{res}\sqrt{\varepsilon_0\varepsilon_c\mu_0}} \tag{1}$$

The patch length is denoted as L_P, μ_0 signifies free space permeability, and ε_0 signifies free space permittivity, while ε_C represents permittivity of Rogers RT/duroid 5880 substrate. f_{res} denotes patch antenna resonant frequency, which will be discussed shortly.

($\varepsilon_0 = 8.85 \times 10^{-12}$ Fm^{-1} and $\mu_0 = 1.257 \times 10^{-6}$ Hm^{-1})

2.2 Effective length of proposed patch

$$L_{ef} = L_P + 2\Delta L_P \tag{2}$$

The patch antenna effective length is represented as L_{ef}. This is of utmost importance as the effect of fringing (Balanis 2016) makes the patch a touch larger than its actual length virtually, when compared to its tangible dimensions. ΔL_P is the add-on length of patch antenna.

2.3 Length extension of proposed patch

Like mentioned earlier, the fringing phenomenon makes the antenna enhance its length of the patch.

$$\Delta L_P = t(0.412)\frac{(\varepsilon_{ref} + 0.3)}{(\varepsilon_{ref} - 0.258)}\left(\frac{\frac{wd}{t} + 0.264}{\frac{wd}{t} + 0.8}\right) \tag{3}$$

ΔL_P symbolizes a slight amendment in patch length that occurs as a result of the fringing process (Balanis 2016). The width of patch and substrate thickness are symbolised by wd and t separately, in the preceding equation.

2.4 Calculation of resonant frequency

$$f_{res} \approx \frac{c}{2L_P\sqrt{\varepsilon_c}} \tag{4}$$

In the preceding equation, f_{res} denotes resonant frequency and ε_c as mentioned earlier denotes permittivity of Rogers RT/duroid 5880 substrate, having value 2.2.

2.5 Effective permittivity

$$\varepsilon_{ref} = \frac{\varepsilon_c + 1}{2} + \frac{\varepsilon_c - 1}{2}\left[1 + 12\left(\frac{t}{wd}\right)\right]^{-1/2} \tag{5}$$

The effective permittivity of the antenna afterwards, when the fringing process has been finally completed (Balanis 2016) at the end, ends up being ε_{ref} like shown in the preceding equation.

2.6 Bandwidth calculation for the antenna

In general, narrow bandwidth is a major problem when we consider the case of any normal patch antenna. In our case, we have been able to generate a fairly broader bandwidth % after performing several iterations by altering the antenna dimensions like length and width of patch, height of the substrate and several other factors as well, which we will discuss in detail in Sect. 3.1 (ref. Fig. 3a)

$$BW\% = \frac{f_H - f_L}{f_C} \tag{6}$$

where, BW% = Bandwidth %, f_H = peak frequency at − 10 dB return loss point, f_L = starting frequency at − 10 dB return loss point, f_C = center frequency of the patch antenna.

2.7 Inductance for coaxial cable

The inductance for coaxial cable is not just dependant on the material's dielectric constant encompassed by the pair of conductors, and is related to the logarithmic value of ratio between the conductor couple.

$$I = 0.459 log_{10}\left(\frac{Do}{di}\right) \tag{7}$$

where, I = Coaxial cable Inductance in μH.m^{-1}, Do = Diameter of external conductor, di = Diameter of internal conductor.

2.8 Impedance for coaxial cable

The impedance for coaxial cable is primarily obtained from the internal and external conductor diameters. Aside from this, the dielectric constant is responsible in ascertaining the characteristic impedance.

$$Z_{ch} = (138\, log_{10}(Do/di))/\sqrt{\varepsilon_c} \tag{8}$$

where, Z_{ch} = characteristic impedance of coaxial cable in ohms.

2.9 Velocity of signal through coax cable

With regards to movement in free space, the signal velocity when passing through a medium (V_m) changes in an inverse manner with respect to square root of ε_c.

$$V_m = \frac{1}{\sqrt{\varepsilon_c}} \tag{9}$$

2.10 Evaluation of antenna radiation pattern

In order to compute the approximate strength of electric field in far field region of the antenna, an equivalent magnetic current line source is assigned at an arbitrary point (Kanda 1990) on the periphery of the patch ($\vec{p}_l$).

$$\vec{p}_l = t\widehat{no}x\vec{F}|_b \tag{10}$$

where, the electric field inside the microstrip cavity (when cavity model is considered) (Palanisamy and Garg 1986) is symbolised as $\vec{F}$, $\widehat{no}$ is the normal which is assumed from patch boundary in the plane of the patch, pointing to the

outward direction and x represents the axis on which the normal is taken. The patch boundary, that is represented by b, is present in z = 0 plane, where t represents substrate thickness.

Electric vector potential $\vec{V}$ in region of far-field is computed with the help of the following equation (Sarkar et al. 2019).

$$\vec{V}(r,\theta,\Phi) = \frac{-2e^{-jk_0 r}}{4\pi r} \int_{-\infty}^{\infty} \iint \vec{k}(x,y,z) \, e^{jk_0(x\cos\phi\sin\theta + y\sin\phi\sin\theta + z\cos\theta)} dxdydz \tag{11}$$

where k_0 denotes free-space wave number and r, θ, Φ denote the spherical polar coordinates, where r is the distance from the origin, θ is the angle from the polar direction and Φ is azimuthal angle. The three axes of the cartesian coordinate system are represented by x, y and z. The components of the electric field are accomplished as follows (Werner 2018),

$$F_\theta = k_0\left(-V_x \sin\Phi + V_y \cos\Phi\right) \tag{12}$$

$$F_\Phi = -k_0\left(-V_x \cos\Phi + V_y \sin\Phi\right)\cos\theta \tag{13}$$

A decent antenna radiation pattern is a key performance parameter in determining how well an antenna performs. A symmetric pattern of radiation would mean that the antenna radiates well uniformly across all directions. This factor is in addition to the fact, that a patch antenna generates a wideband performance because of change in the antenna height and substrate thickness. The E-field and H-field radiation patterns for the proposed antenna can be seen in Fig. 6a and b, respectively.

3 Design and simulated results of the antenna

In order to propagate the impedance bandwidth, the desired patch antenna is designed by placing symmetrically a couple of opposite-faced U-slots, located equidistantly from the center as given in Fig. 1. The antenna has a size of (l × w = 38 mm × 35 mm) and it is placed upon a substrate that comprises of Rogers RT/duroid 5880 material. It possesses a height of 3.14 mm. The lower part of the substrate is coated with perfect electric conductor (PEC), which behaves like a ground plane. The size of the substrate is l × w × h = 95 mm × 95 mm × 3.14 mm. It is made to feed coaxially with the help of a couple of 50-Ω probes that have the same magnitudes. In order to maintain the symmetry of radiation patterns, the couple of probes should be located at equal distances from the patch centre as demonstrated in Figs. 1 and 2. It must be noted that the

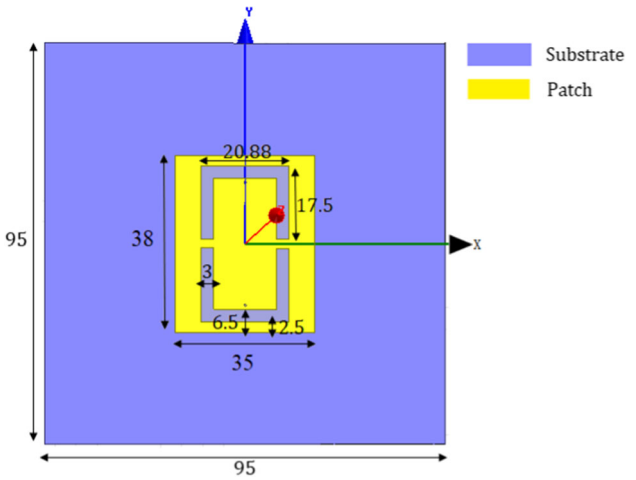

Fig. 1 Top view of patch antenna design

asymmetric placement of probes severely affects impedance bandwidth.

The notable characteristic of the proposed antenna, is that it creates a decent range of bandwidth around a particular resonant frequency, interestingly whose value matches exactly with the patch antenna centre frequency i.e., 3 GHz along with having a fairly good impedance match. In addition to this, the patterns of radiation that are acquired, are perfectly symmetrical which indicates that an ideal balance is retained between coaxial probe-pair, and are equi-distant from patch centre.

3.1 Influence on bandwidth through change in antenna parameters

In general, we know that the amendment in length of patch produces shifting in resonant frequency at the output end. A several number of iterations were considered to validate this point. Additionally, certain iterations were also taken care of, where the patch width was modified and thickness of substrate was changed, but the material of the substrate was kept unchanged. A comparative analysis was done for all the parameters with respect to the proposed parameters and a final comparison was done altogether in a graph in order to keep a close eye on where exactly these changes are taking place.

In this case, we are dealing with 3 dB bandwidth, where comparisons were done for the various values for separate iterations with respect to the proposed parameters. As the name indicates, bandwidth of the frequencies for all the iterations were evaluated over a range of 3 dB where the starting and ending values of that range were examined for the desirable resonant frequency. Upon examining the various iterations in Fig. 3b with the modified parameters, a gradual variation is visible in the position of each and

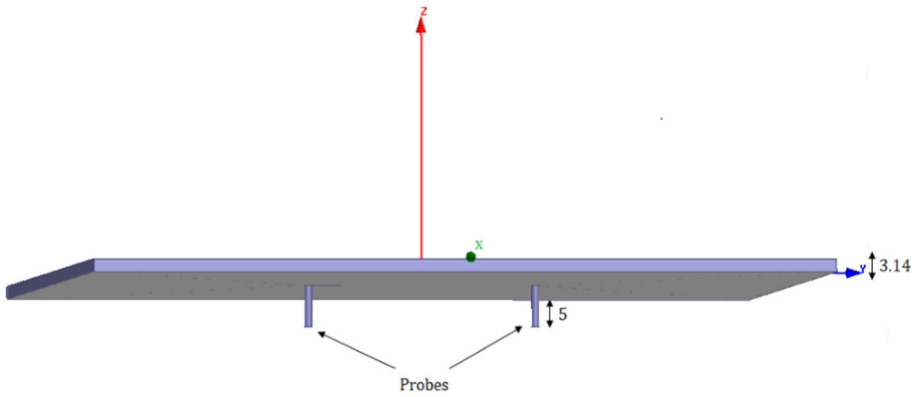

Fig. 2 Side view of patch antenna design

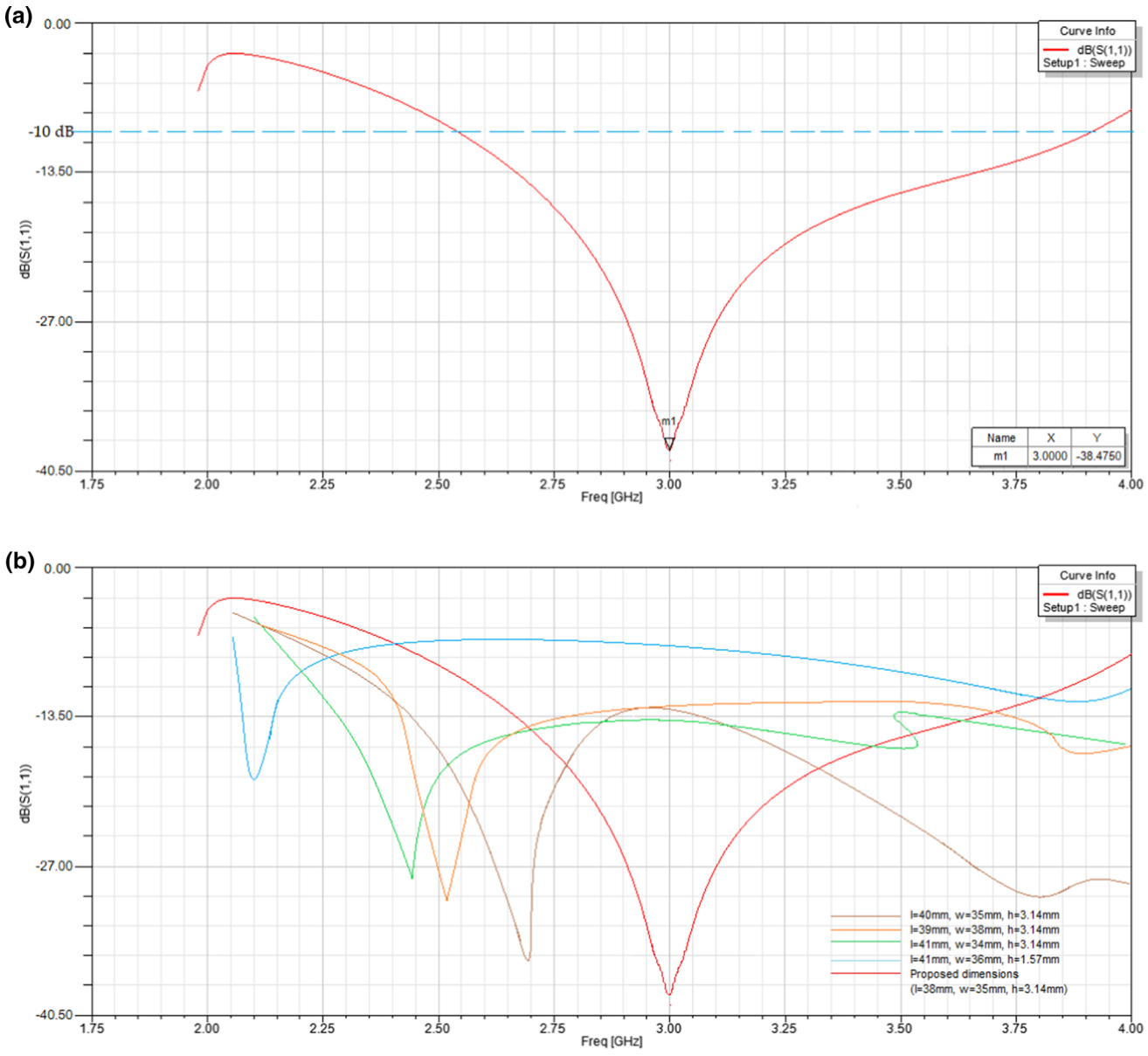

Fig. 3 **a** Impedance bandwidth of the antenna. **b** 3 dB Bandwidth analysis of antenna via amendment of specific antenna dimensions

every resonant frequency as they move nearer to 3 GHz, which is the design centre frequency.

From the readings, it can be observed that position of resonant frequency for the proposed antenna in Fig. 1, matches exactly with the antenna centre frequency at 3 GHz. This antenna design has minimal losses as it is clear from the reflection coefficient value in the graphical analysis, after comparison with each and every iteration. This even suggests that the impedance match for the antenna proposed is nearly perfect and this explains the decent value of bandwidth. Furthermore, from the graph it can be seen that − 10 dB impedance bandwidth range of the proposed antenna, starts from 2.54 GHz and ends at 3.91 GHz, and its value in % turns out to be 45.67 (ref. Eq. 6) as seen from Fig. 3a.

3.2 Influence on impedance in Smith chart

The amendment in the antenna dimensions too has a say on the impact of impedance on Smith chart. It contributes importantly to the impedance match of an antenna. It is not that hard to determine that the name, Smith chart, originates from the name of its inventor, Phillip Smith, who had founded it around the 1940s. It's a renowned mechanism for measuring the input impedance and is very widely used for this purpose. Even though, its application is a little less now, after different simulation softwares have come into existence, but despite that, it is significant in its own way as we can see from Fig. 4a and b, for the determination of input impedance.

3.3 Influence on electric field distribution of patch

The distribution of electric field also varies based on the adjustments done to the parameters as visible in Fig. 5a–d. An interesting thing to note is, as we slowly move further from the patch centre towards the slot boundaries, the value of electric field keeps escalating further. Although, the reading at mid-point of the patch is nearly zero and additionally, the subsequent area adjacent to the slots also have no magnitude. Thus, it can be said that changes in the electric field only occurs within the area adjacent to the slots and does not take place anywhere else. Figure 5e shows field distribution of proposed antenna.

3.4 Influence on radiation pattern of antenna

The amendment of the patch parameters also brings about variations in the field radiation patterns. From Fig. 6c, it is seen that different E-field radiation patterns of several iterations are analysed. It is seen that; these field patterns slowly move nearer towards the field pattern of the antenna with the proposed dimensions. Determining an antenna radiation pattern is key in analysing the measure of performance of an antenna and more symmetric the pattern, the better will be its radiation. A peak radiation intensity value of 14 dB is achieved for 0^{o} as seen in Fig. 6c apart from it being purely symmetric. Figure 6a and b show E and H field radiation patterns and its importance in judging the antenna bandwidth is discussed in Sect. 2.10.

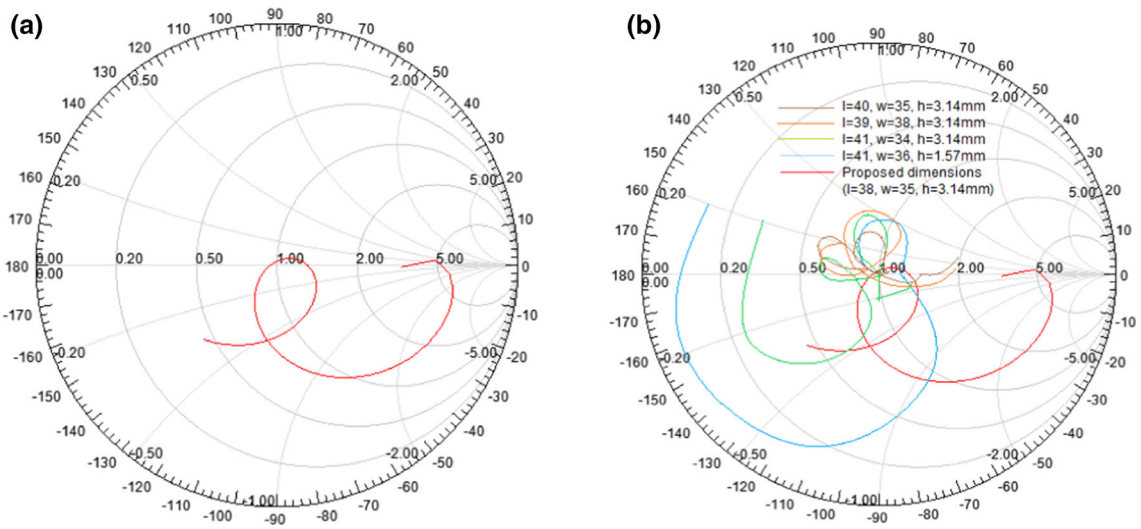

Fig. 4 **a** Input impedance in Smith chart for the antenna **b** Analyzing input impedance via amendment of specific dimensions of the antenna

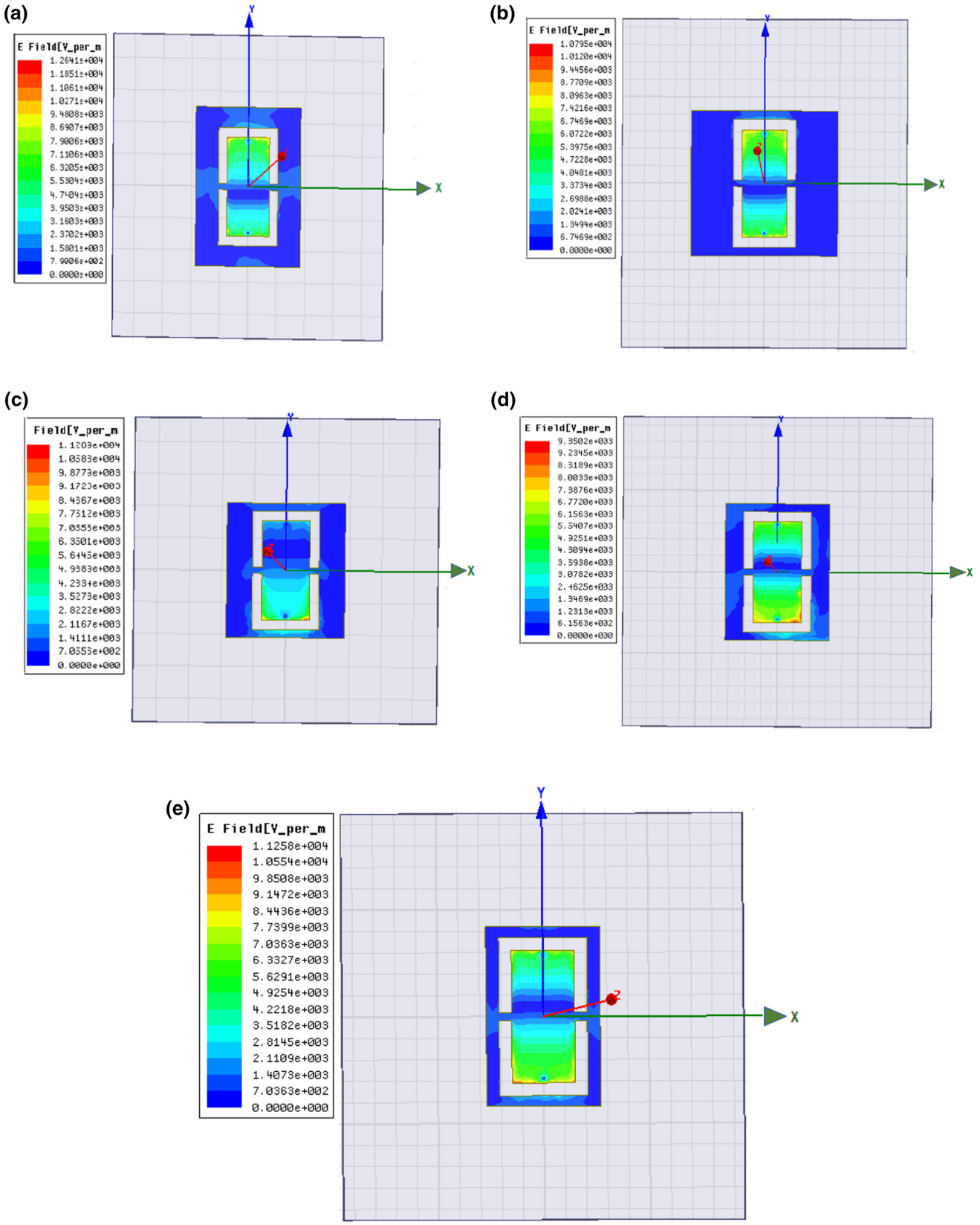
(a)
E Field[V_per_m
1.2641e+004
1.1851e+004
1.1061e+004
1.0271e+004
9.4808e+003
8.6907e+003
7.9006e+003
7.1106e+003
6.3205e+003
5.5304e+003
4.7404e+003
3.9503e+003
3.1603e+003
2.3702e+003
1.5801e+003
7.9006e+002
0.0000e+000
Y
X
(b)
E Field[V_per_m
1.0795e+004
1.0120e+004
9.4456e+003
8.7709e+003
8.0963e+003
7.4216e+003
6.7469e+003
6.0722e+003
5.3975e+003
4.7228e+003
4.0481e+003
3.3734e+003
2.6988e+003
2.0241e+003
1.3494e+003
6.7469e+002
0.0000e+000
Y
X
(c)
Field[V_per_m
1.1203e+004
1.0583e+004
9.8773e+003
9.1720e+003
8.4367e+003
7.7312e+003
7.0555e+003
6.3501e+003
5.6445e+003
4.9388e+003
4.2334e+003
3.5273e+003
2.8222e+003
2.1167e+003
1.4111e+003
7.0553e+002
0.0000e+000
Y
X
(d)
E Field[V_per_m
9.3502e+033
9.2345e+033
8.5189e+033
8.0033e+033
7.3876e+033
6.7720e+033
6.1563e+033
5.5407e+033
4.9251e+033
4.3094e+033
3.5938e+033
3.0782e+033
2.4625e+033
1.8469e+033
1.2313e+033
6.1563e+032
0.0000e+030
Y
X
(e)
E Field[V_per_m
1.1258e+004
1.0554e+004
9.8508e+003
9.1472e+003
8.4436e+003
7.7399e+003
7.0363e+003
6.3327e+003
5.6291e+003
4.9254e+003
4.2218e+003
3.5182e+003
2.8145e+003
2.1109e+003
1.4073e+003
7.0363e+002
0.0000e+000
Y
X

◀**Fig. 5** **a** Analysis of electric field distribution of antenna having dimensions l = 40 mm, w = 35 mm, h = 3.14 mm; **b** Analysis of Electric field distribution of Antenna having dimensions l = 39 mm, w = 38 mm, h = 3.14 mm; **c** Analysis of Electric field distribution of Antenna having dimensions l = 41 mm, w = 34 mm, h = 3.14 mm; **d** Analysis of Electric field distribution of Antenna having dimensions l = 41 mm, w = 36 mm, h = 1.57 mm; **e** Electric field distribution of the Patch Antenna with proposed dimensions (l = 38 mm, w = 35 mm, h = 3.14 mm)

3.5 Gain and VSWR plot

The gain and VSWR plots with respect to frequency are observed from Figs. 7 and 8 respectively. While noticing Fig. 7, we see a gain of close to 6 dB is achieved for our desired structure for the center frequency of 3 GHz. It's an acceptable value with regards to Bluetooth and also WLAN networks. Referring to the VSWR graph in Fig. 8, it is seen that a value of 1.03 is achieved which is quite close to an ideal VSWR value. Generally, its value must be below 2, only then we can say that the antenna has a good impedance match. Precisely, it should lie as near as possible to 1. So, its value should lie in between 1 and 2 for an almost perfect match, whereas if VSWR exceeds 2, then it would suggest improper matching of the input and output terminals of the antenna.

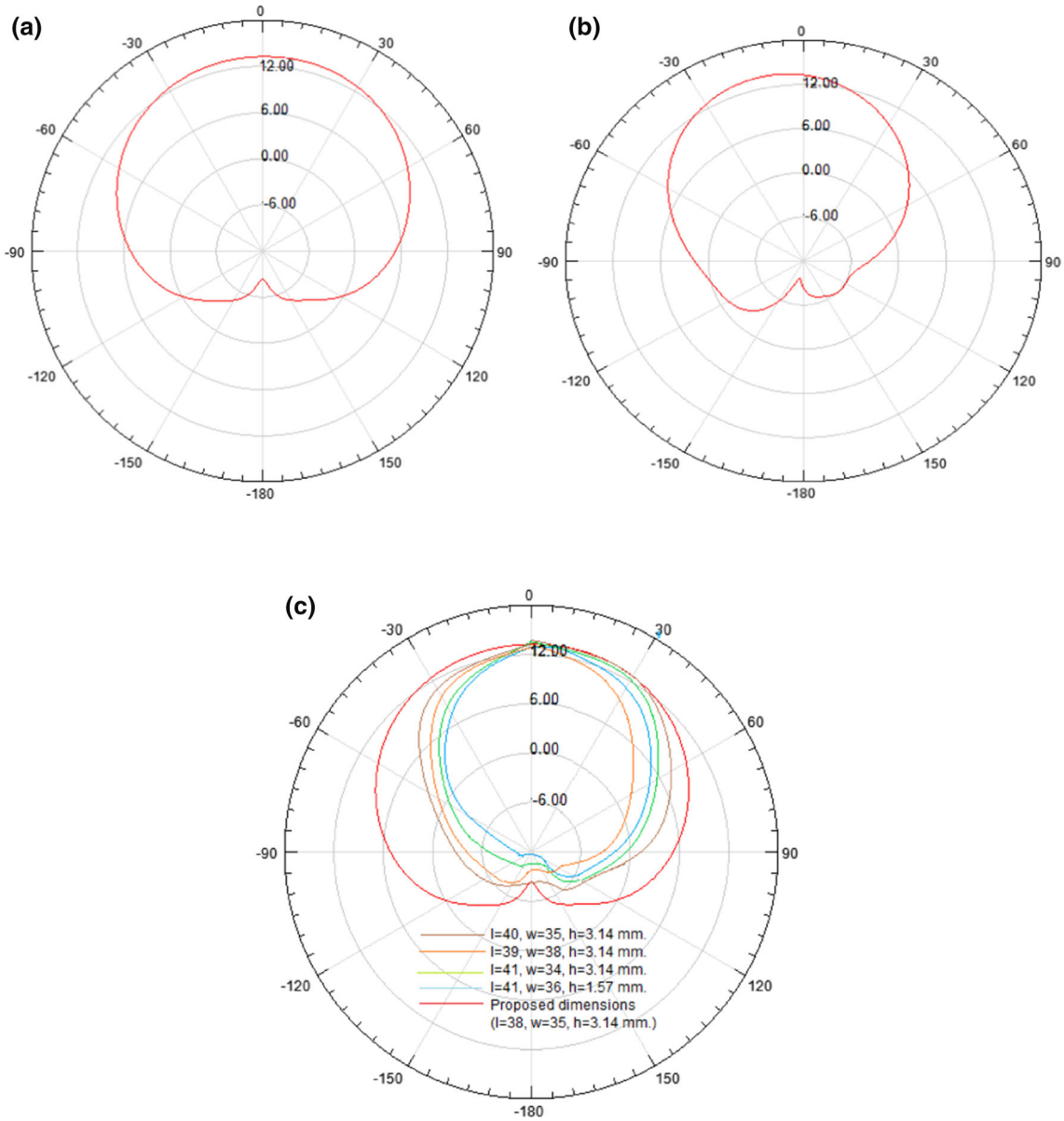

Fig. 6 **a** E-field antenna radiation pattern; **b** H-field antenna radiation pattern **c** Analysis of E-field antenna radiation pattern having specified antenna dimensions

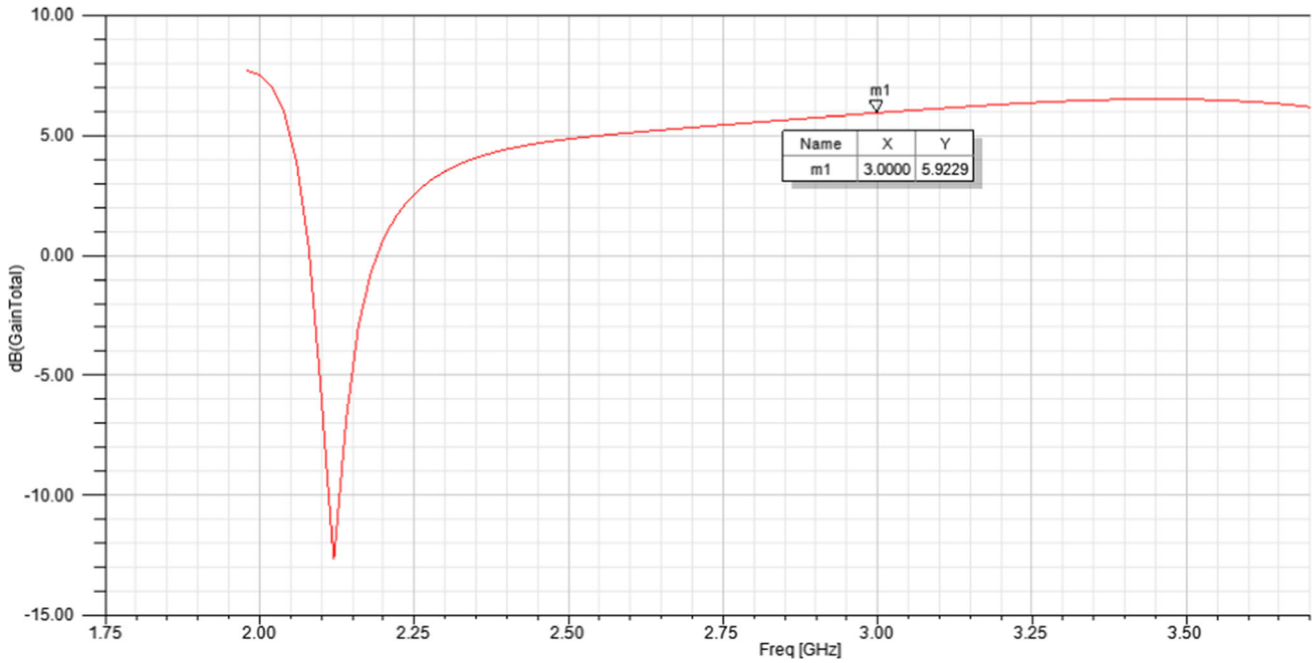

Fig. 7 Gain vs freq for proposed antenna with value at center frequency = 3 GHz

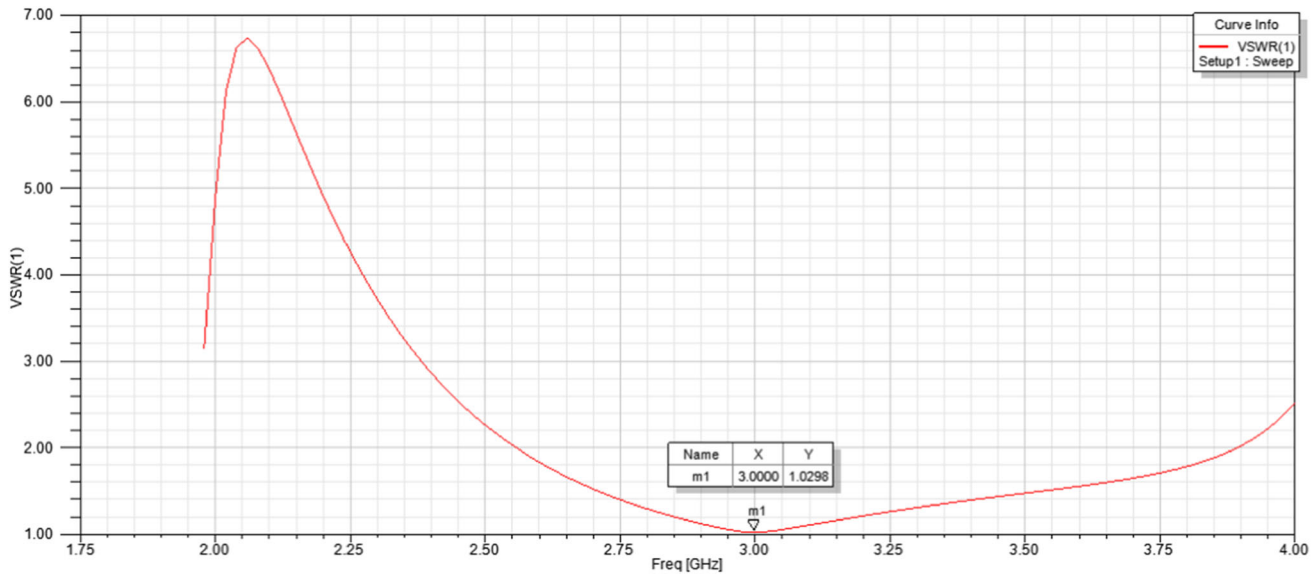

Fig. 8 VSWR graph of the antenna proposed (value can be seen very near to 1)

3.6 Comparative study of antenna parameters

Figure 9 shows the Bar graph comparison of the different 3 dB bandwidths with respect to the bandwidth of the proposed resonant frequency. The readings are correlated alongside the measurements of our desired patch antenna in order to check the measure of bandwidth improvement occurring for each resonant frequency. While referring to Fig. 3b, it is seen that the alteration in the parameters causes the resonant frequency for each of the iterations to move closer to the patch antenna center frequency. The most enhanced bandwidth of all the iterations (other than proposed value) that we obtain is 70 MHz for 2.52 GHz of resonant frequency, while the least value that we obtain is 37.5 MHz for a resonant frequency having value 2.69 GHz. The value of bandwidth for proposed dimensions of the antenna at 3 GHz is 100 MHz. It is to be noted that, the improvement in the bandwidth for the 3 GHz centre frequency is zero in the mentioned figure. This is because, the bandwidth at 3 GHz frequency matches identically with the bandwidth at the antenna center frequency, which is 3 GHz as well. Therefore, as both

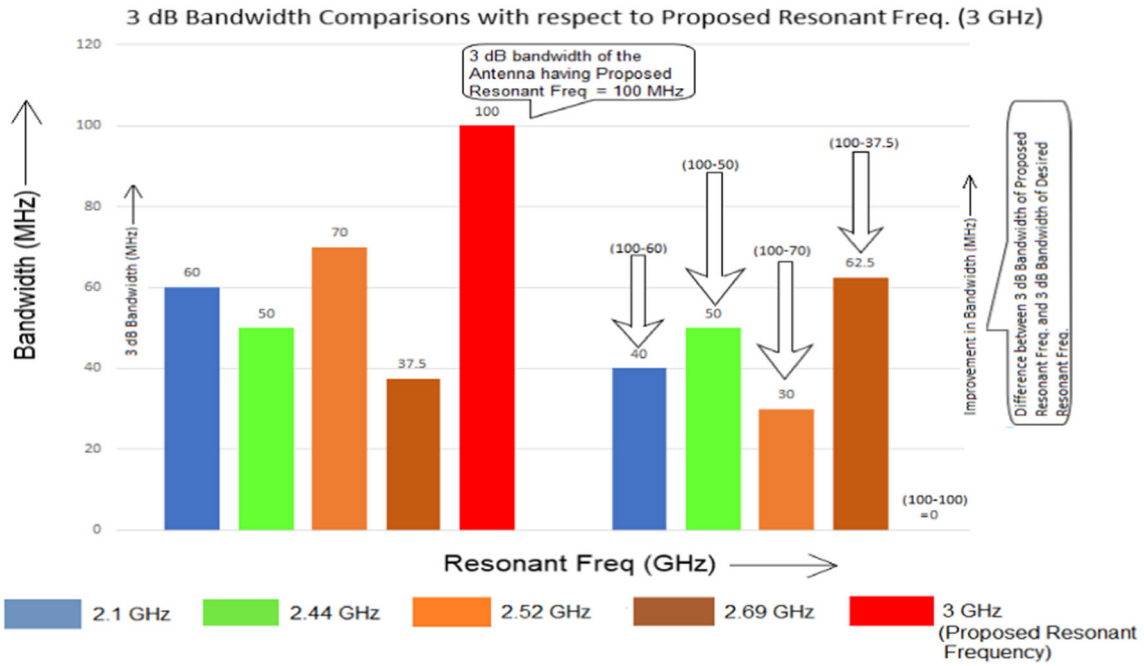

Fig. 9 Bar graph analysis of 3 dB antenna bandwidth

Table 1 Comparative study of Antenna Parameters between proposed work and various published articles

Refs.	Op. freq (GHz)	VSWR	Radiation intensity (dB)	Radiation pattern symmetry
(Lee et al.2010)	3	1.6	6 ($\theta = 0^0$)	✘
(Alani et al. 2020)	3	1.22	5 ($\theta = 0^0$)	✘
(Radavaram et al. 2019)	3	1.05	8 ($\theta = 0^0$)	✔
(Mahbub et al. 2021)	3	1.07	12.7 ($\theta = 0^0$)	✔
(Ghaffar et al. 2021)	3	1.8	10 ($\theta = 0^0$)	✘
Proposed antenna	3	1.03	14 ($\theta = 0^0$)	✔

bandwidths are identical at that same frequency of 3 GHz, the improvement in bandwidth for that particular frequency is zero as seen in Fig. 9. The impedance match of the proposed antenna is decent when we consider 1.03 as VSWR value. In ideal cases, 1 signifies perfect matching of an antenna. And normally, decent impedance matching would mean that VSWR value must be below 2. Furthermore, a gain close to 6 dB was achieved for our desired structure at 3 GHz of center frequency. Thus, it can be said that our proposed antenna has a good wideband performance within the range of S-band (2–4 GHz) and is ideally suited to that frequency range.

A detailed analysis was done on the various parameters on patch antenna in Table 1 and these were compared with recent relevant studies to check their variations of different parameters like VSWR, radiation intensity and radiation pattern symmetry. While referring to Table 1, it will be seen that the greatest value of radiation intensity achieved is

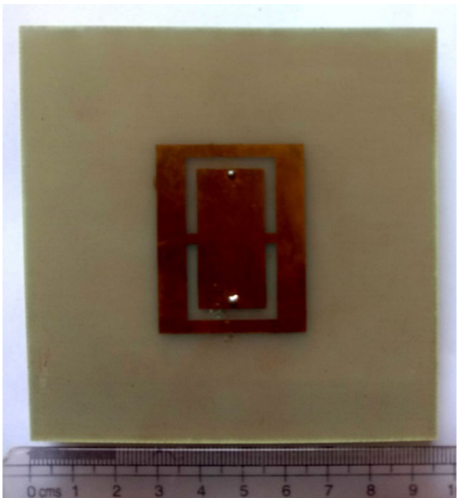

Fig. 10 Fabricated prototype of proposed structure

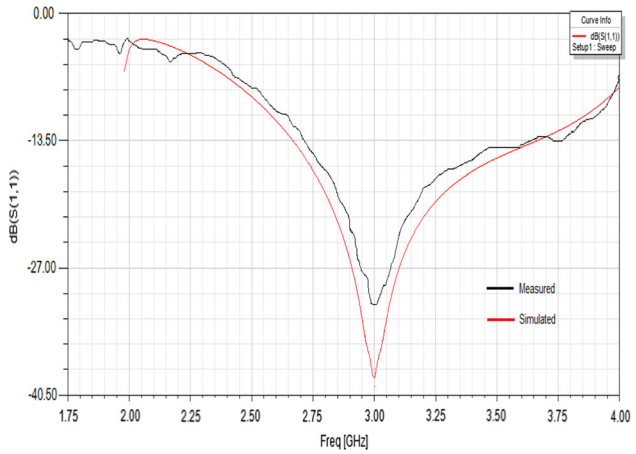

Fig. 11 Comparison between the results of the values of measurement and simulation for the reflection coefficient of the proposed model

14 dB at 0° for our desired structure with the least VSWR value of 1.03 along with symmetric radiation pattern.

4 Fabricated antenna design

The patch antenna fabricated model is seen in Fig. 10 that has identical dimensions like the one used for simulation. It was initially modelled with the help of Ansoft HFSS and that was followed by printing the design on the surface of a glossy paper. After that, this part of the design was extracted and put on top of a Rogers-RT/duroid 5880 substrate having proposed measurements. Chemical etching procedure was then applied for eliminating the surplus metal surrounding the substrate in such a manner that only the design portion is left intact.

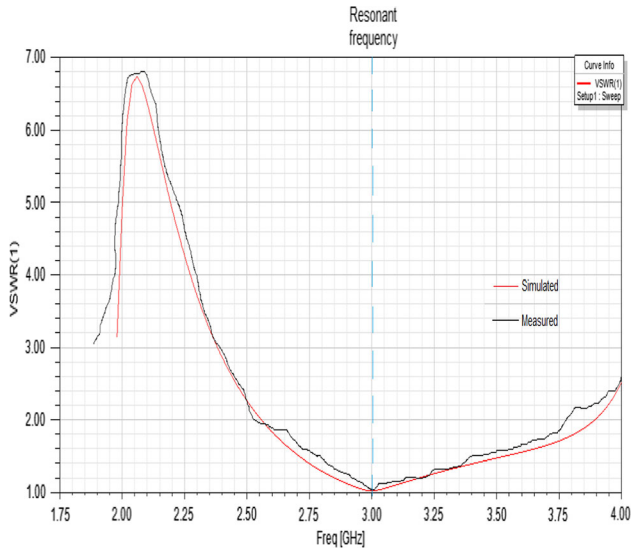

Fig. 12 Comparison between the Results of the values of measurement and simulation for the VSWR of the proposed model

Some variations are noticeable when simulated and measured results are compared as observed in Figs. 11 and 12. These probably take place as a result of the consequences of the soldering process in the fabricated structure.

As it can be seen from Fig. 11, the simulated value of the reflection coefficient for the proposed antenna is − 38.48 dB. Whereas when observe the measured value graph, the value of reflection coefficient is then − 31.05 dB. Likewise in Fig. 12, the difference in values of measurement and simulation is visible from the VSWR plot. From the simulated result, we can see that graph of VSWR is almost 1 at 3 GHz frequency, where the value 1 indicates a perfect match. But in this case, as it can be seen, the measured value is almost at a close proximity to the simulated one for 3 GHz.

5 Conclusion

It is well known that narrow bandwidth is quite an area of concern with regards to patch antennas that hinders their long-term performances. For our case, increment in bandwidth was done for a particular resonant frequency, incidentally that resembles the antenna center frequency of 3 GHz besides having a formidable impedance match. The same was obtained via inclusion of a slot-couple on the patch in addition to having a couple of probes and besides that, a few mathematical iterations were performed on the measurements of the patch. This process was continued and eventually our proposed model was designed, and for a certain resonant frequency of 3 GHz, an impedance bandwidth of 45.67% was achieved, which is more than what a conventional patch antenna would generate at this frequency range of 2–4 GHz (S-band). In addition to this, purely symmetric field radiation pattern of antenna was achieved with a formidable radiation intensity having 14 dB as its value at 0° with a VSWR of 1.03. A potentially high gain of 5.92 dB was achieved with regards to the above-mentioned range of frequency, and all of these factors combined make our antenna a really good candidate for wideband generation within that frequency range. Also simulated results are in good compatibility with the measured values.

Funding This research is not funded by any funding agency.

Data availability Not applicable as no datasets were analysed during this research.

Code availability Not applicable.

Declarations

Conflict of interest The authors declare that they have no conflicts of interest.

References

AL-Amoudi MA (2021) Study, design, and simulation for microstrip patch antenna. Int J Appl Sci Eng Rev (IJASER) 2(2):1–29

Alani S, Zakaria Z, Ahmad A (2020) Miniaturized UWB elliptical patch antenna for skin cancer diagnosis imaging. Int J Electric Comput Eng 10(2):1422

Ashraf S (2020) Culminate coverage for sensor network through Bodacious-instance mechanism. Wireless Commun and Mobile Comput. https://doi.org/10.26634/jwcn.8.3.17310

Ashraf S, Gao M, Chen Z, Naeem H, Ahmad A, Ahmed T (2020) Underwater pragmatic routing approach through packet reverberation mechanism. IEEE Access 8:163091–163114

Ata OW, Salamin M, Abusabha K (2020) Double U-slot rectangular patch antenna for multiband applications. Comput Electr Eng 84:106608

Balanis CA (2016) Antenna theory: analysis and design. John Wiley & Sons

Bansal A, Gupta R (2020) A review on microstrip patch antenna and feeding techniques. Int J Inf Technol 12(1):149–154

Baudha S, Basak A, Manocha M, Yadav MV (2020) A compact planar antenna with extended patch and truncated ground plane for ultra wide band application. Microw Opt Technol Lett 62(1):200–209

Cai L, Wong H, Tong KF (2020) A simple low-profile coaxially-fed magneto-electric dipole antenna without slot-cavity. IEEE Open J Antennas Propag 1:233–238

Cendes Z (2016) The development of HFSS. In: 2016 USNC-URSI Radio Science Meeting, IEEE, pp 39–40

Chen W, Lee KF, Lee RQ (1993) Spectral-domain moment-method analysis of coplanar microstrip parasitic subarrays. Microw Opt Technol Lett 6(3):157–163

Coax Impedance: Coaxial Cable Characteristic Impedance: Available online from https://www.electronics-notes.com/articles/antennas-propagation/rf-feeders-transmission-lines/coaxial-cable-characteristic-impedance.php

Deshmukh AA, Chavali VA, Ambekar AG (2021) Wideband designs of offset U-slot and dual U-slot cut rectangular microstrip antennas. In: 2021 4th Biennial International Conference on Nascent Technologies in Engineering (ICNTE), IEEE, pp 1–6

Dhara R, Yadav S, Sharma MM, Jana SK, Govil MC (2021) A circularly polarized quad-band annular ring antenna with asymmetric ground plane using theory of characteristic modes. Prog Electromagn Res M 100:51–68

Gaharwar M, Dhubkarya DC (2021) X-band multilayer stacked microstrip antenna using novel electromagnetic band-gap structures. IETE J Res. https://doi.org/10.1080/03772063.2021.1883484

Gao S, Lin H, Ge L, Zhang D (2019) A magneto-electric dipole antenna with switchable circular polarization. IEEE Access 7:40013–40018

Ghaffar A, Li XJ, Awan WA, Iffat Naqvi S, Hussain N, Seet BC, Limiti E (2021) Design and realization of a frequency reconfigurable multimode antenna for ISM, 5G-sub-6-GHz, and S-band applications. Appl Sci 11(4):1635

Gopi D, Vadaboyina AR, Dabbakuti JRK (2021) DGS based monopole circular-shaped patch antenna for UWB applications. SN Appl Sci 3(2):1–12

Goudos SK Siakavara, K, Kalialakis C (2017) Application of Opposition-Based Learning concepts for arbitrary patch antenna design for wireless communications. In: 2017 International Workshop on Antenna Technology: Small Antennas, Innovative Structures, and Applications (iWAT), IEEE, pp 171–174

Guo YX, Luk KM, Lee KF, Chow YL (1998) Double U-slot rectangular patch antenna. Electron Lett 34(19):1805–1806

He Y, Li Y (2020) Dual-polarized microstrip antennas with capacitive via fence for wide beamwidth and high isolation. IEEE Trans Antennas Propag 68(7):5095–5103

Jung YJ, Choi HK, Yu BA, Kim J, Lee C, Ahsan MS, Sohn IB (2020) Femtosecond laser-assisted fabrication of microstrip patch antenna. Opt Eng 59(9):096103

Kanda M (1990) A microstrip patch antenna as a standard transmitting and receiving antenna. IEEE Trans Electromagn Compat 32(1):5–8

Kaur A, Malik PK (2021) Multiband elliptical patch fractal and defected ground structures microstrip patch antenna for wireless applications. Prog Electromagn Res B 91:157–173

Khan M, Chatterjee D (2016) Characteristic mode analysis of a class of empirical design techniques for probe-fed, U-slot microstrip patch antennas. IEEE Trans Antennas Propag 64(7):2758–2770

Lee RQ, Lee KF, Bobinchak J (1987) Characteristics of a two-layer electromagnetically coupled rectangular patch antenna. Electron Lett 23(20):1070–1072

Lee KF, Yang SLS, Kishk AA, Luk KM (2010) The versatile U-slot patch antenna 52:1 (71–88). IEEE Antennas Propag Mag 52(2):5525569 (**Erratum**)

Mahbub F, Akash, SB, Al-Nahiun SAK, Islam R, Hasan RR, Rahman MA (2021) Microstrip Patch Antenna for the Applications of WLAN Systems using S-Band. In: 2021 IEEE 11th Annual Computing and Communication Workshop and Conference (CCWC), IEEE, pp 1185–1189

Mak CL, Lee KF, Luk KM, Kishk AA (2003) Half U-slot patch antenna with shorting wall. Electron Lett 39(25):1

Mishra R, Kuchhal P, Kumar A (2015) Effect of height of the substrate and width of the patch on the performance characteristics of microstrip antenna. Int J Electric Comput Eng 5(6):1441

Naz F, Umrani FA, Soomro ZA, Ali Z, Hafeez S (2020) Comparative analysis of symmetrical and the asymmetrical golden ratio U slot microstrip patch antenna. In: 2020 3rd International Conference on Computing, Mathematics and Engineering Technologies (iCoMET), IEEE, pp 1–5

Nguyen MT, Lin YF, Chang CH, Chen CH, Chen HM (2021) Compact shorted C-shaped patch antenna for ultrahigh frequency radio frequency identification tags mounted on a metallic plate. Int J RF Microwave Comput Aided Eng 31(6):e22595

Ou JH, Huang J, Liu J, Tang J, Zhang XY (2020) High-gain circular patch antenna and array with introduction of multiple shorting pins. IEEE Trans Antennas Propag 68(9):6506–6515

Palanisamy V, Garg R (1986) Analysis of arbitrarily shaped microstrip patch antennas using segmentation technique and cavity model. IEEE Trans Antennas Propag 34(10):1208–1213

Prajapati M, Rawat A (2020) Performance analysis of IRNSS using compact microstrip patch antenna for S band application. Acta Geophys 68(4):1223–1228

Prakasam V, LaxmiKanth KA, Srinivasu P (2020) Design and simulation of circular microstrip patch antenna with line feed wireless communication application. In: 2020 4th International Conference on Intelligent Computing and Control Systems (ICICCS), IEEE, pp 279–284

Radavaram S, Pour M (2019) Wideband radiation reconfigurable microstrip patch antenna loaded with two inverted U-slots. IEEE Trans Antennas Propag 67(3):1501–1508

Saini GS, Kumar R (2021) A low profile patch antenna for Ku-band applications. Int J Electron Lett 9(1):47–57

Sarkar D, Mikki SM, Antar YM (2019) An efficient analytical evaluation of the electromagnetic cross correlation green's

function in MIMO systems. IEEE Trans Antennas Propag 67(11):6947–6956
Sharma SK, Shafai L (2009) Performance of a novel ψ -shape microstrip patch antenna with wide bandwidth. IEEE Antennas Wirel Propag Lett 8:468–471
Sun JN, Li JL, Xia L (2019) A dual-polarized magneto-electric dipole antenna for application to N77/N78 band. IEEE Access 7:161708–161715
Weigand S, Huff GH, Pan KH, Bernhard JT (2003) Analysis and design of broad-band single-layer rectangular U-slot microstrip patch antennas. IEEE Trans Antennas Propag 51(3):457–468
Werner DH (2018) Exact expressions for the far-zone electromagnetic fields radiated by thin elliptical loop antennas of arbitrary size. IEEE Trans Antennas Propag 66(12):6844–6850
Yang F, Zhang XX, Ye X, Rahmat-Samii Y (2001) Wide-band E-shaped patch antennas for wireless communications. IEEE Trans Antennas Propag 49(7):1094–1100
Yunas J, Yunu NHM, Sampe J, Nandiyanto AB (2020) Design and fabrication of glass based mems patch antenna for energy harvester. In: 2020 IEEE international conference on power and Energy (PECon), IEEE, pp 362–365